Abstract

From conformational analysis, we have determined the two lowest energy crystal structures for the hard segments of 4,4'-diphenylmethane diisocyanate/1,4-butanediol (MDI/BDO)-based polyurethane elastomer. Both crystal forms give prominent X-ray scattering at ~7.6 Å. In one crystal form, (1), there is strong hydrogen bonding between linear chains with a density of 1.30 g/cm^3, while in the other form, (2), van der Waals bonding gives rise to a double helix structure with a density of 1.22 g/cm^3 and a formation energy 1.6 kJ/mol higher than form (1). The double helix crystal has a unit cell length of 18.8 Å which is about half the 34.7 Å unit cell length of the hydrogen-bonded crystal. The X-ray diffraction predicted for each crystal is presented and compared with experiment.

Keywords: atomistic modeling; conformational analysis; hard segments; polyurethane elastomer; X-ray diffraction

Conformational Analysis of the Crystal Structure for MDI/BDO Hard Segments of Polyurethane Elastomers

CHRIS W. PATTERSON, DAVID HANSON, ANTONIO REDONDO, STEPHEN L. SCOTT, NEIL HENSON

Theoretical Division, Los Alamos National Laboratory, Los Alamos, New Mexico, 87544

Received 10 November 1997; revised 17 May 1999; accepted 18 May 1999

ABSTRACT: From conformational analysis, we have determined the two lowest energy crystal structures for the hard segments of 4,4′-diphenylmethane diisocyanate/1,4-butanediol (MDI/BDO)-based polyurethane elastomer. Both crystal forms give prominent X-ray scattering at ~7.6 Å. In one crystal form, (1), there is strong hydrogen bonding between linear chains with a density of 1.30 g/cm^3, while in the other form, (2), van der Waals bonding gives rise to a double helix structure with a density of 1.22 g/cm^3 and a formation energy 1.6 kJ/mol higher than form (1). The double helix crystal has a unit cell length of 18.8 Å which is about half the 34.7 Å unit cell length of the hydrogen-bonded crystal. The X-ray diffraction predicted for each crystal is presented and compared with experiment. © 1999 John Wiley & Sons, Inc. J Polym Sci B: Polym Phys 37: 2303–2313, 1999

Keywords: atomistic modeling; conformational analysis; hard segments; polyurethane elastomer; X-ray diffraction

INTRODUCTION

Polyurethane elastomers, based on the hard segment 4,4′-diphenylmethane diisocyanate (MDI) and 1,4-butanediol (BDO) denoted by MDI/BDO, have been extensively studied by X-ray scattering techniques to determine the possible crystal structures. Early, wide-angle X-ray studies by Bonart et al.[1–3] showed an off-meridian reflection at about 7.9 Å, some 30° from the fiber axis. Bonart et al. proposed that the hydrogen bonding between fibers caused the fibers to be staggered resulting in the alignment of the amine and carbonyl groups. Such packing is indeed seen in model compounds where the crystal structure can be determined unambiguously.[4–6] Wide-angle X-ray studies of oriented thin films of MDI/BDO have been ambiguous, leading to a number of different proposed triclinic crystal structures all resulting in staggered chains presumed to arise from hydrogen bonding.[7–11] The densities of these proposed hard segment crystals range from 1.32 to 1.58 g/cm^3 compared to the experimental determination[10,12] of 1.25–1.35 g/cm^3. Part of the problem of assigning a unique crystal structure from a given wide-angle X-ray pattern is that the hard segments of MDI/BDO are paracrystaline and give rise to only a few broad diffraction lines for which assignments are ambiguous. Thus, the same or similar diffraction patterns have led to different crystal assignments by different investigators.

This problem is compounded by the fact that there have been no determinations of the structure factors for the X-ray fiber patterns, and investigators have not been able to show that the given assignments actually correspond to the most intense scattering. Any complete analyses of the wide-angle X-ray results must also explain the absence of Bragg lines in the data. For any assignment made, there are typically hundreds of lines of the same scattering order that are not visible in the diffraction pattern, a point usually ignored by previous investigators. For example,

Correspondence to: A. Redondo (E-mail: redondo@lanl.gov)

Journal of Polymer Science: Part B: Polymer Physics, Vol. 37, 2303–2313 (1999)
 CCC 0887-6266/99/172303-11

Table I. Configuration Energies (kJ/mol) and Crystal Structures for Various Geometries of MDI/BDO (HB = Hydrogen Bonded)

	1. Single Strand	2. HB Dimer a-axis	3. HB Dimer b-axis	4. Double Helix Dimer	5. Unconnected HB Crystal	6. Connected HB Crystal	7. Double Helix Crystal
Bonded interactions							
Bond stretching	171.6	338.6	338.2	339.1	159.1	159.5	160.7
Bond bending	108.8	210.6	219.3	218.5	106.7	105.5	105.9
Torsional energy	3.8	30.6	19.3	16.3	40.6	37.3	15.9
Total bonded	284.2	579.8	576.8	573.9	306.4	302.3	282.5
Nonbonded interactions							
vdW repulsion	1117.7	2381.8	2377.6	2451.3	1492.3	1511.1	1466.4
vdW dispersion	−529.5	−1370.5	−1368.4	−1511.1	−1369.2	−1378.9	−1339.9
Coulomb energy	−555.1	−1134.8	−1145.7	−1112.2	−592.7	−583.5	−570.6
Total nonbonded	33.1	−123.5	−136.5	−172.0	−469.6	−451.3	−444.1
Total energy	317.3	456.3	440.3	401.9	−163.2	−149.0	−161.6
Crystal structure							
a (Å)					6.72	6.64	7.26
b (Å)					5.66	5.60	8.59
c (Å)					36.68	34.73	18.77
ρ (g/cm^3)					1.27	1.30	1.22
α					113.3°	108.6°	54.3°
β					61.3°	68.1°	93.5°
γ					132.8°	132.8°	82.7°

all investigators have assigned the 7.6–7.9 Å scattering feature to the (004) Bragg diffraction, yet there is no explanation for why the (001), (002), (003), and (005) diffraction peaks are never seen. This is particularly striking because there does not appear to be any selection rule due to crystal symmetry that would eliminate any of these lines (as, for example, one would find in body-centered and face-centered cubic crystals). Furthermore, there is no explanation for why the Bragg lines at (h00) and (0k0) are apparently never seen, although they should be quite intense. For these reasons, we believe it is important to show the fiber diffraction pattern resulting from a proposed crystal assignment so that the absence of predicted features in the data becomes obvious.

The task of deducing the crystal structure from a diffraction pattern is aggravated by the fact that it is now known that the hard segments can occur in several crystal forms.[13–15] It is not known precisely which wide-angle X-ray diffraction patterns correspond to which crystal forms or even how many crystal forms may actually be expressed in the data. Wide-angle X-ray studies by Briber and Thomas[13] have shown the appearance of at least three different types of paracrystals. Type I is found in unstretched samples, Type II in stretched samples, and Types II and III occur upon stretching and annealing. Thus, Type III is included in all the previous wide-angle X-ray studies of oriented and annealed thin films and may itself actually correspond to more than one crystal form. No determination of the crystal structure has been attempted for Types I and II. Briber and Thomas[13] found that Type III has a more extended fiber than Type II, which corresponds to a 4.6 Å line, in agreement with Blackwell and Lee.[14]

Alternatively, Koberstein and Stein[16] have interpreted small-angle X-ray data to conclude that the hard segment microdomains of MDI/BDO are in sheets (laminae) only a few MDI units thick as a result of considerable chain folding. This is in contrast to the original model of Bonart in which connected chains are held together by hydrogen bonding.

Finally, we should mention that differential scanning calorimetry thermograms[14,17] show hard segment crystal endotherms at two different temperatures which could be attributed to the presence of two different crystal forms. Apparently, the lower temperature endotherm is associated with the extended crystal Type III form. Overall, we conclude that there is considerable confusion in the determination of crystal structure from X-ray scattering data for MDI/BDO polyurethane hard segments.

In this paper, we shall attempt to determine the possible crystal structures of MDI/BDO hard segments by conformational analysis. There have been numerous conformational studies of the MDI/BDO molecules comprising the crystal.[6,18–21] Previous investigators, however, did not determine crystal structure by energy minimization because of the large number of atoms in the unit cell and the computational difficulty in obtaining convergence for van der Waals and Coulomb energies between cells. In this paper, we use the well-documented commercial software packages InsightII® and Discover® from Molecular Simulations Inc.[22] to accomplish this task. The use of a widely available commercial software package makes it possible for anyone to repeat the calculations with the same standard molecular potentials. Further, this code has been benchmarked for numerous other molecular crystals and its accuracy documented in the literature.[22] In the next section, we describe the procedure we used to minimize the energies of the molecular dimers and the molecular crystals of MDI/BDO in both the hydrogen-bonded and double helix conformations. Then, we give the results of the energy minimization for the dimers followed by the results for the crystal. Finally, we discuss the crystal fiber X-ray spectra resulting from the two crystal forms found previously.

METHOD FOR ENERGY MINIMIZATION

The MSI InsightII® code assigns an empirical potential energy function to each atom from the *cvff* forcefield[22] depending on the element type and the nature of the chemical bond. The total bond energy includes the bond stretching, bond bending, and bond torsion (dihedral angle) terms. Empirical partial charges are assigned to each of the atoms with the total molecular charge being zero. Consequently, part of the intramolecular energy minimization includes the electrostatic Coulomb potential between atoms. Empirical van der Waals potentials, which include repulsive and dispersive terms, are also assigned to each pair of atoms. The total nonbond energy is the sum of the Coulomb and van der Waals energies. In Table I, we show the various potential energies for the MDI/BDO minimum configuration.

These calculations, in agreement with Blackwell et al.,[19,20] indicate that the energy minimum for MDI/BDO corresponds to all *trans* carbon bonds in the BDO segment as shown in Figure 1. Furthermore, the urethane group of the MDI is in the same plane with the nearest benzene ring as previously noted.[21] The benzene rings in the MDI segments form planes which intersect at 90°. For the minimum energy configuration, the urethane bonds occur on alternate sides of the benzene rings for each MDI unit and on alternate sides of the BDO link between MDI units. In Figure 1, we have used two MDI units and have artificially truncated the polymer chain with hydrogens after two carbons of the BDO extender. This comprises the unit cell in a hydrogen-bonded crystal, and we shall use this unit for comparison. This model unit can be readily extended to make the hydrogen-bonded crystal by deleting the terminal hydrogens. The energy minimization calculations for the conformation shown in Figure 1 are in complete agreement with previous conforma-

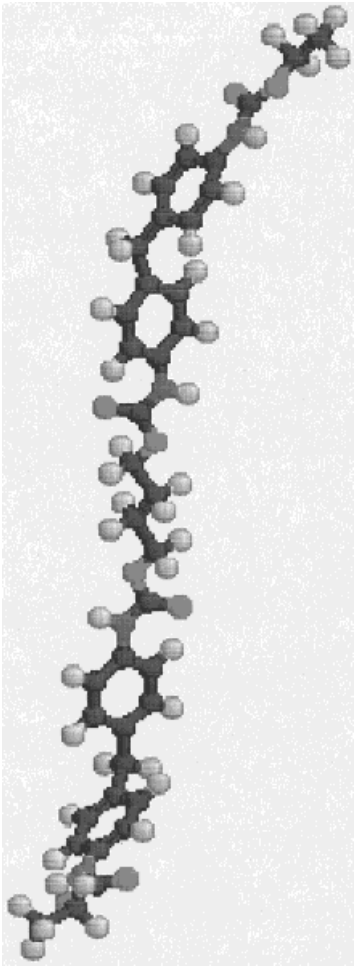

Figure 1. Strand of MDI/BDO containing two MDI units used to build the crystal cell. The ends are capped with hydrogens when the cells are unconnected. Energies are given in Table I (column 1).

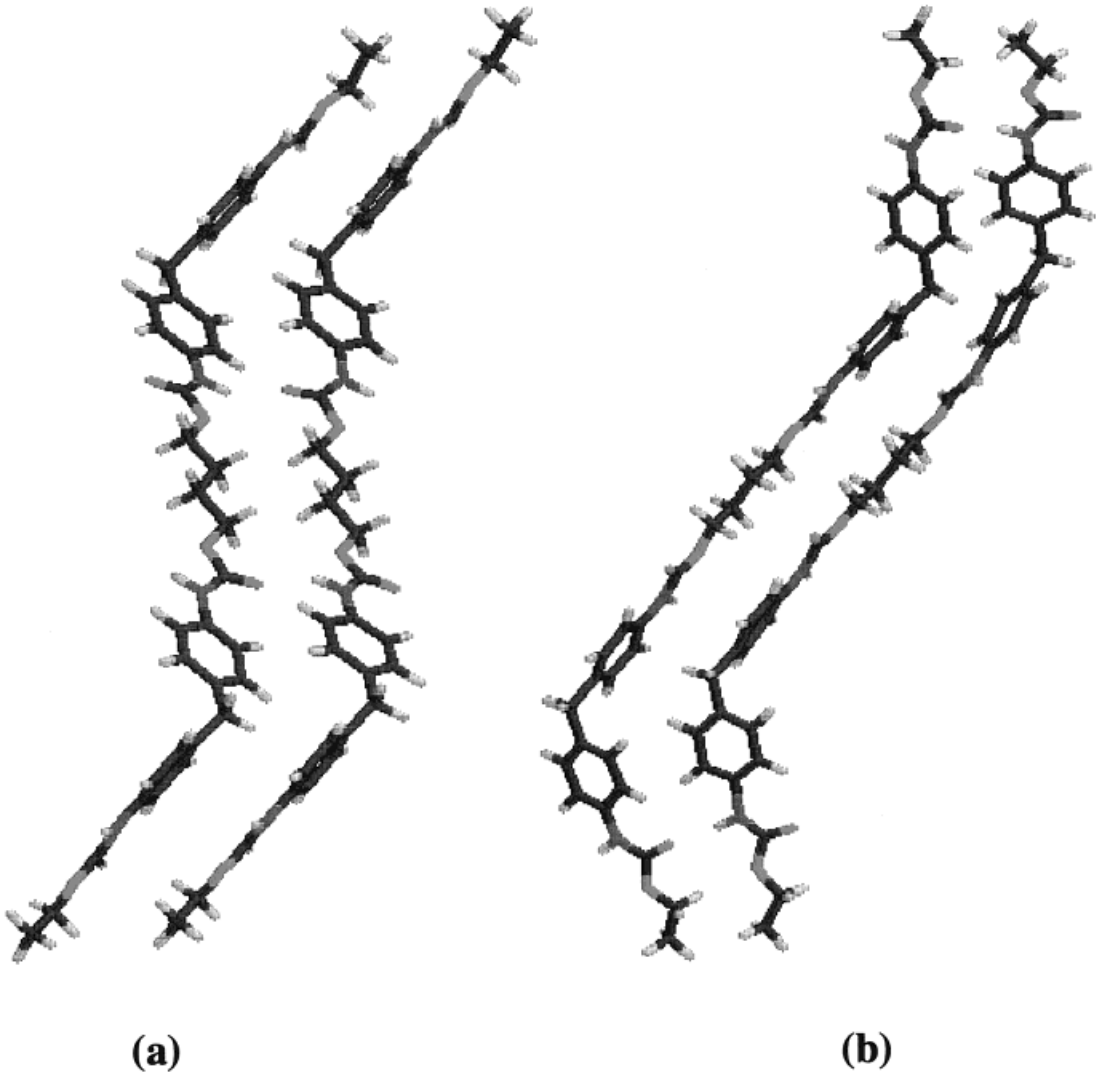

Figure 2. Dimers formed from the single strands shown in Figure 1. The hydrogen bonding of the strands occurs along two different axes corresponding to (a) and (b) only to the extent that the benzene rings are in the same plane. Energies are given in Table I (columns 2–3).

tional analyses of MDI/BDO which have been reported by numerous authors.[18–21] The energies for this MDI/BDO unit are shown in Table I (column 1).

In this work, we are interested in the dimer and crystal conformations that arise from interactions between MDI/BDO molecules and chains. These interactions are entirely due to nonbonding and electrostatic interactions that are treated in the crystal energy minimization using Ewald summation methods. In practice, it is necessary to try many initial configurations of the molecular MDI/BDO and crystal unit cells in order to sample the large configuration space. The MSI InsightII® program will alter the crystal parameters and the molecular bonds in order to minimize the energy. The minimizations were performed at constant pressure with all degrees of freedom allowed to relax. Still, the two lowest energy configurations found were at least 20 kJ/mol below all others. To accomplish the minimizations, it is much easier to leave the strands unconnected and unbonded lengthwise between adjacent cells in order to sample configuration space rapidly and to observe where the molecular ends prefer to go. The resulting geometry then suggests the connectivity between cells to form the linear chains.

MOLECULAR MDI/BDO DIMERS

Bonart[1–3] originally proposed by that the MDI/BDO chain was staggered about 30° in the crystal in order to accommodate the hydrogen bonding between the NH and OC in the urethane bond. The staggering actually occurs in both axes perpendicular to the chain axis. In order to show this, we exhibit the dimer configuration corresponding to the energy minimum for the crystal a- and b-axes, respectively [see Fig. 2(a) and (b)]. The staggering is evident in both Figure 2(a) and (b) where the alignment of NH and OC between molecules occurs twice in each figure for each MDI/BDO molecule, corresponding to the two different sets of planes containing the benzene rings in MDI. In Table I (columns 2–3) we compare the energies for the two hydrogen-bonded configurations shown in Figure 2.

The energy of the hydrogen-bonded dimer in Figure 2(b) is 16 kJ/mol lower than that of the hydrogen-bonded dimer in Figure 2(a). The interaction energy is dominated by the van der Waals energy between the benzene rings and the Coulombic hydrogen bonding. The maximum van der Waals energy between two adjacent benzene rings is about 20 kJ/mol, similar to that of a hydrogen bond. However, it is much easier to align the two planes of the benzene rings than the two axes of the NH and OC. For this reason, the dimer configuration which minimizes the energy is mostly determined by the alignment of the benzene rings, leading to similar contributions to the total energy in both Figure 2(a) and (b), as shown in Table I (columns 2–3). The energy for Figure 2(b) is somewhat lower because the urethane bonds at the ends of the molecules can bend to align the NH and OC. In Figure 2(a), the urethane bonds are in the middle of the molecules and alignment is poor because the urethane bonds are not in the same plane.

The minimum energy configuration for the dimer, however, is formed by a double helix geometry of the two MDI/BDO chains shown in Figure 3. To our knowledge, this has not been previously reported The individual strands in Figure 3 are the same as in Figures 1 and 2, except the BDO chain extender has one gauche bond between the middle two carbon atoms. The gauche bond requires an additional 15 kJ/mol of energy. However, this energy penalty is more than compensated by the nearly perfect alignment of the benzene rings resulting in a lower van der Waals energy. In Table I (column 4), we find that the energy for the double helix dimer is 38.4 kJ/mol lower than that for the hydrogen-bonded dimer shown in Figure 2(b). Despite the additional 15 kJ/mol of energy for the carbon gauche bond, the total energy due to bonded interactions for the double helix dimer is even lower than the hydrogen-bonded strand dimer in Figure 2(b) by 2.9 kJ/mol. This is because the double helix has much less distortion of the bond and dihedral angles to accommodate the benzene ring interactions. In fact, the total energy due to bonded interactions

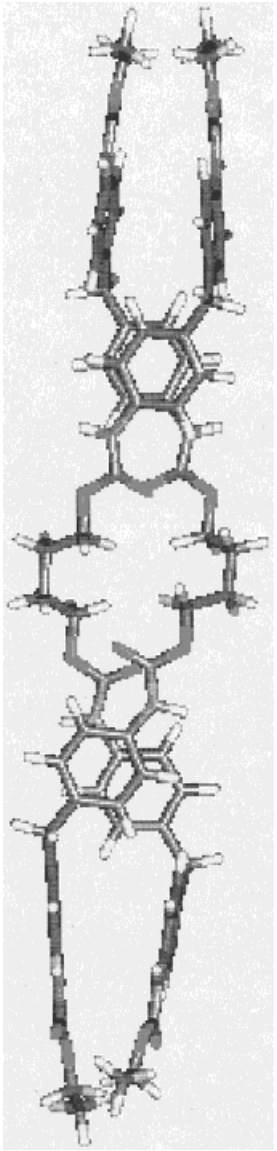

Figure 3. Dimer formed from two strands intertwined in a double helix. Because the benzene rings of the diphenylmethane are facing each other in the two strands, there is no hydrogen bonding. Energies are given in Table I (column 4).

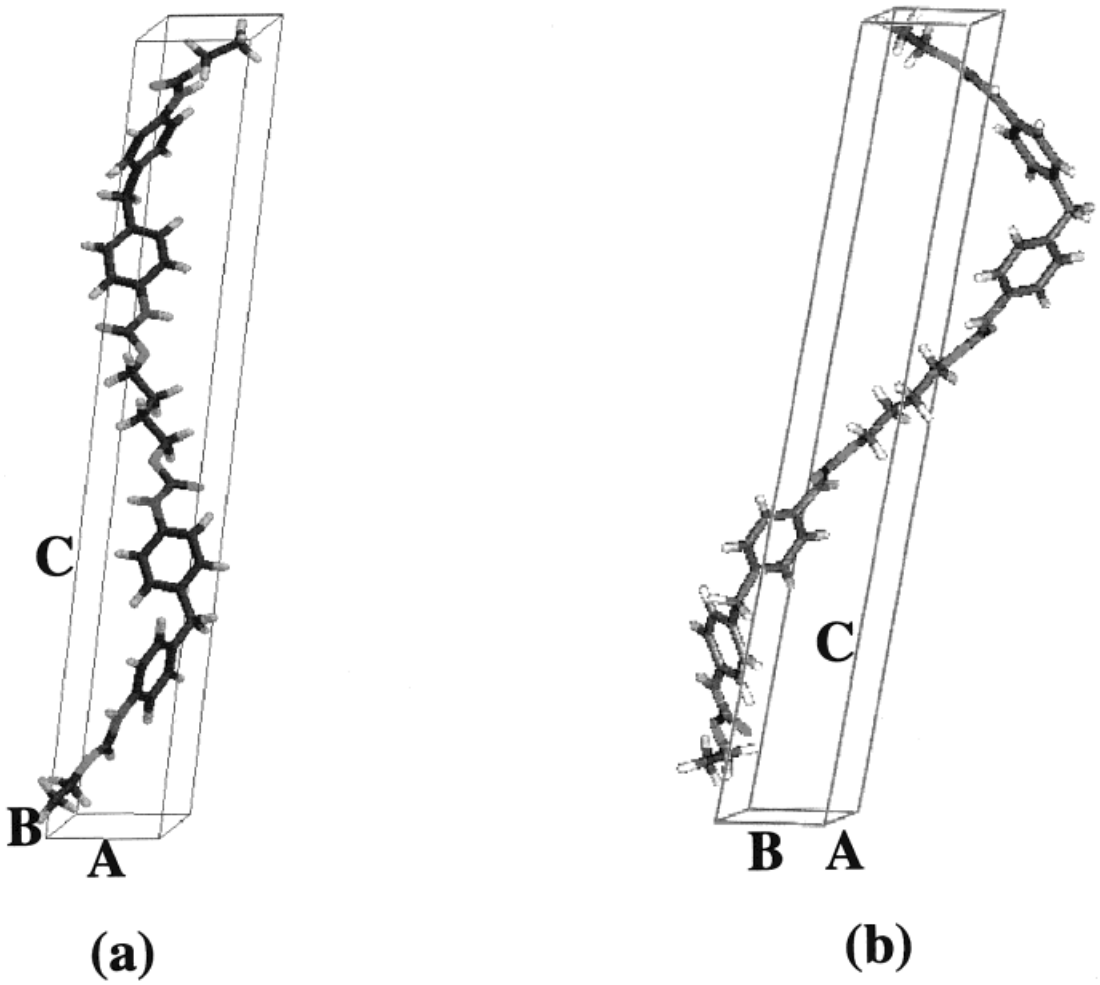

Figure 4. Crystal made from unconnected single strands with hydrogen bonding between cells. (a) View along the b-axis; (b) view along the a-axis. Energies and crystal structure are given in Table I (column 5).

when molecules are separated remains at 573.9 kJ/mol, so there is virtually no distortion of the molecules as they form the double helix dimer. By contrast, the bonded interaction energy of the hydrogen-bonded dimer in Figure 2(b) is 8.4 kJ/mol higher than that for the separated molecules.

There is no hydrogen bonding in the double helix because the urethane bonds for the two molecules are always in parallel planes separated by about 4 Å. Thus, as Table I (columns 2, 3 and 4) show, the Coulomb contribution to the total energy for the double helix dimer in Figure 3 is 23–34 kJ/mol higher than that of the hydrogen-bonded dimers in Figure 2. However, because of the excellent alignment of the benzene rings, the van der Waals contribution (repulsive and dispersive) to the total energy for the double helix dimer is 69–71 kJ/mol lower than that of the hydrogen-bonded dimers. For connected chains, the energy differences between the two dimers are multiplied by the number of pairs of MDI units in each chain.

HARD SEGMENT MDI/BDO CRYSTAL STRUCTURE

We now compare the crystal energies for the hydrogen-bonded and double helix conformations and determine the X-ray fiber pattern for the resulting crystals. Although the double helix configuration has a lower energy than the hydrogen-bonded dimer, *this is not the case for the crystal*. In the crystal, the hydrogen bonds of the single strand will occur along both transverse crystal axes, not just in one direction as for the dimer. As

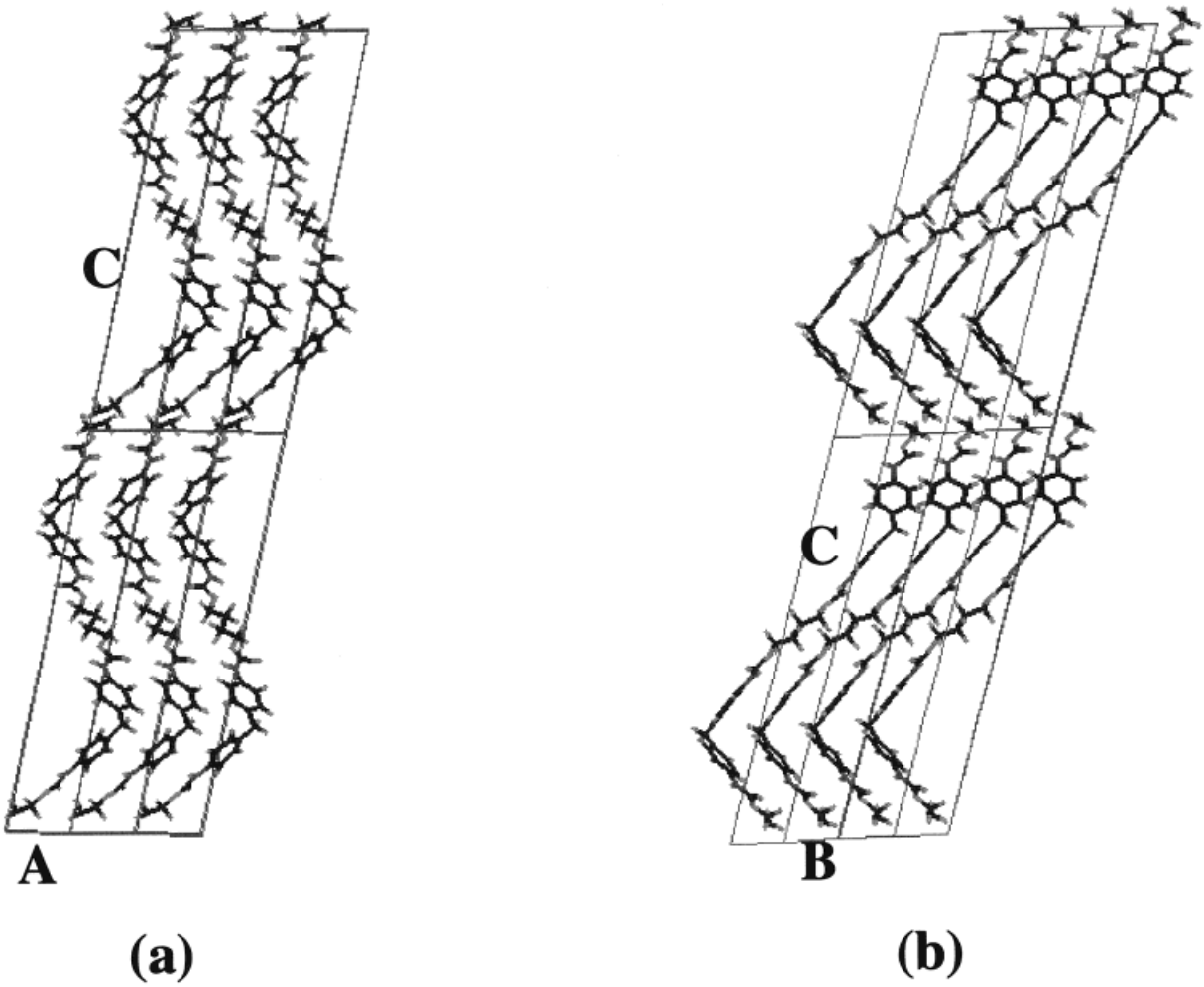

Figure 5. Crystals made from connected single strands with hydrogen bonding between cells. Strands are connected in adjacent b-cells. (a) View along the b-axis; (b) view along the a-axis. Energies and crystal structure are given in Table I (column 6).

a result, we find the hydrogen-bonded crystal energy is 1.6 kJ/mol lower than the double helix crystal, a value less than the accuracy of the code. The energies and crystal parameters for the hydrogen-bonded unconnected chains are given in Table I (column 5). In Figure 4, we show the hydrogen-bonded crystal conformation in the unconnected chain in which there are only two MDI units. From this figure, it is seen that the chain is most readily extended along the c-direction within the same cell along the a-axis, but in an adjacent cell along the b-axis. Thus, the fiber axis will not be along the c-axis, but slightly tilted toward the b-axis which is 132.8° from the c-axis.

With this information, we now connect the molecules in the unit cells in the manner suggested by Figure 4 to determine the hydrogen-bonded connected chain crystal cell conformation. The energies and crystal parameters for this hydrogen-bonded conformation are given in Table I (column 6). Note that, with their ends constrained, the energy for the hydrogen-bonded connected chain is higher by 14.2 kJ/mol than the hydrogen-bonded unconnected chain crystal. The bonded interaction contributions to the total energies stay nearly the same, but the nonbonded energy increases by nearly 18 kJ/mol because the ends of the molecules are joined to the adjacent cell along the c-axis. The principal difference is that the crystal cell shortens in the c-direction because it is now directly bonded to adjacent molecules to form the fiber chain. This connection is shown in Figure 5(a) and (b), which should be compared to the dimers shown in Figure 2(a) and (b), respec-

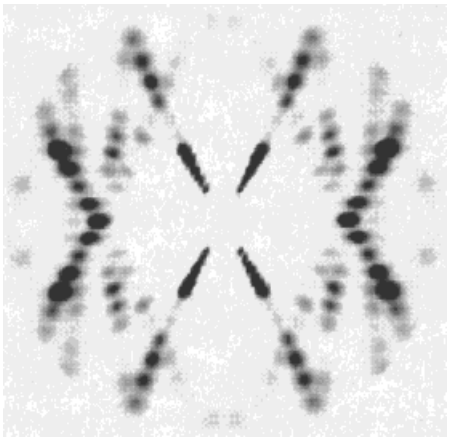

Figure 6. X-ray fiber pattern of crystal made from connected single strands in

tively. As already noted, the hydrogen-bonded dimers do not form in the same plane as their hydrogen bonds and, in fact, the angle between the a- and b-axis, γ, is 132.8° for both the long and short hydrogen-bonded crystal. This large angle is in disagreement with previous crystal structures inferred from the X-ray diffraction assignments. The density of the hydrogen-bonded crystal chain increases from 1.27 to 1.30 g/cm^3 when the strands are connected, which compares favorably with the experimental value[12] of 1.28 g/cm^3.

In Figure 6, we show the calculated X-ray diffraction fiber pattern of the crystal in the conformation of Figure 5. The lowest order diffraction angles and distances for the peaks are summarized in Table II. For ease of calculation, we assumed that the fiber is along the c-axis so that the fiber plot is symmetrical about the horizontal axis. The three progressions of maxima seen in each quadrant are consistent with what is seen in an experimental fiber X-ray diffraction pattern[11] shown in Figure 7. This diffraction pattern was obtained for a MDI-BDO-based polyurethane elastomer containing ~50% hard segments, oriented by stretching 700% and annealed at 130°C for 7 days. The calculated progression (Fig. 6) emanating from the horizontal is quite complicated because of the near overlap of doublets arising from the (-1 0 1) and the (0 -1 1) progressions. Because of this overlap, it is very difficult to derive the crystal structure from the X-ray line positions alone without also comparing the fiber pattern intensities. Also, the progression (10ℓ) occurs near the observed peak at 4.6 Å at about 65° from the vertical. The main discrepancy of this plot with experiment is that the *ab* plane is 23° from the c-axis. As a result, the (004) diffraction peak occurs at 23° rather than the observed value of 37°. The (004) peak also occurs at d = 8.0 Å rather than the observed value of 7.6 Å. Furthermore, the calculated fiber pattern shows diffraction peaks for (001), (002), and (003) which are not seen in experiment, however, these are calculated to be five times weaker than the (004) peak.

In Figure 8, we show the crystal structure for the double helix of unconnected chains and in Table I (column 7), we list the energies and crystal parameters. In comparing the conformational energies of unconnected hydrogen-bonded and double helix crystals (Table I, columns 5 and 7), we see that the Coulomb interaction energy is greater for the double helix structure, a consequence of the absence of hydrogen bonds. On the other hand, the double helix crystal has a lower torsional strain than does the hydrogen-bonded crystal, analogous to the double helix vs. the hydrogen-bonded dimer comparison (Table I, columns 2–3 and 4). We did not determine the con-

Table II. Calculated X-Ray Diffraction Peaks for Conformation of Figure 5

Miller Indices	Distance (Å)	Angle (degrees)
0 01	32.1	23
0 02	16.0	23
0 03	10.7	23
0 04	8.0	23
0 05	6.4	23
0−11	4.1	83
0−12	4.1	76
0−13	3.9	70
0−14	3.8	64
0−15	3.6	59
0 11	4.0	83
0 12	3.9	77
0 13	3.7	71
0 14	3.5	66
0 15	3.3	62
−1 01	4.5	82
−1 02	4.3	76
−1 03	4.0	70
−1 04	3.7	65
−1 05	3.5	60
1 01	4.9	82
1 02	4.9	74
1 03	4.7	66
1 04	4.6	58
1 05	4.3	52

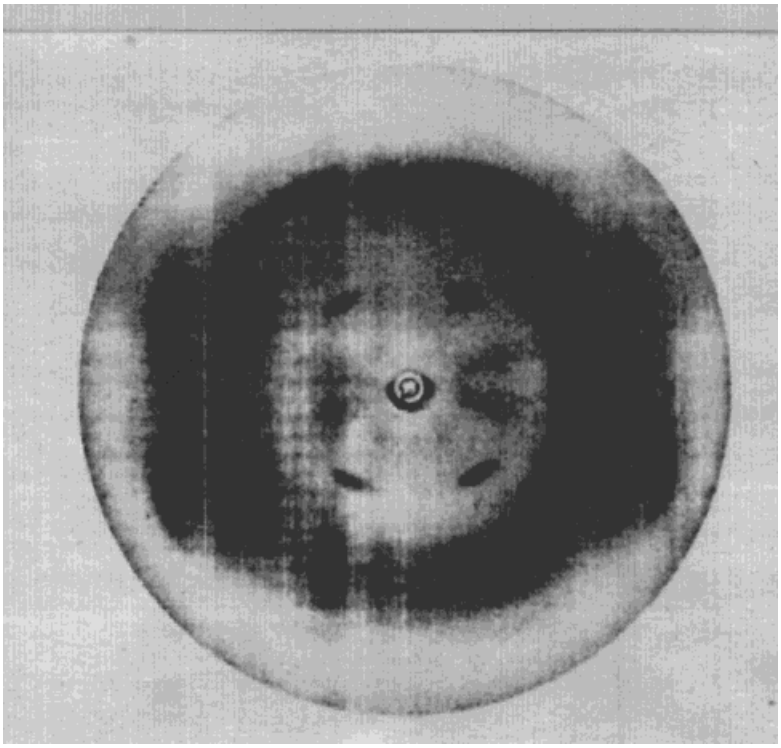

Figure 7. X-ray diffraction photograph for MDI/BDO/PTMA stretched 700% and annealed at 130°C for 7 d (from Ref. 11 with permission).

nected chain crystal because of the difficulty in choosing how the ends of the double helix will connect in adjacent cells. Because of the difficulty in dealing with such a large number of possibilities, this task will be deferred to future work. We would like to stress that the 1.6 kJ/mol energy difference between the unconnected double helix and hydrogen-bonded crystals should not be considered significant since the accuracy of the code is at best about 4 kJ/mol for these types of energy differences.

The fiber diffraction pattern for the unconnected double helix chain is shown in Figure 9. Because the length of the crystal cell for the double helix (18.8 Å) is half that of the hydrogen-bonded cell (34.7 Å), the previous diffraction peaks at (004) and (002) are now equivalent to (002) and (001), and none of the previous odd (00ℓ) are possible. Also, the (002) diffraction is now at 37° with d = 7.5 Å in agreement with experiment. The diffraction peaks at (001) and (002) for the double helix are, by far, the strongest Bragg diffractions. The diffraction progressions near the horizontal are not seen in this case. Assuming the hard segments to be purely of a double helix unconnected chain nature leads to a calculated density of 1.22 g/cm^3, somewhat lower than the experimental value[10,12] of 1.28 g/cm^3. Presumably, the calculated density would increase if the chains were connected

CONCLUSIONS

In this work, we have determined the minimum energy conformations of single chains of MDI/BDO using the Molecular Simulations Inc.[22] codes, and these results are in agreement with those of previous investigators.[18–21] We then found the minimum energy conformations for dimers of MDI/BDO. The lowest energy conformation was found to be a double helix made up of two strands of MDI/BDO with a gauche bond between the middle two carbons of BDO. Despite the 15-kJ/mol energy penalty associated with the gauche bond, the double helix has lower total energy because it enables the two dimethylbenzene rings in each strand to face each other giving rise to a strong van der Waals attraction. We then used the same energy-minimization techniques to determine the lowest two crystal energies of the MDI/BDO hard segments. We computed the fiber X-ray patterns for these two lowest energy crystal

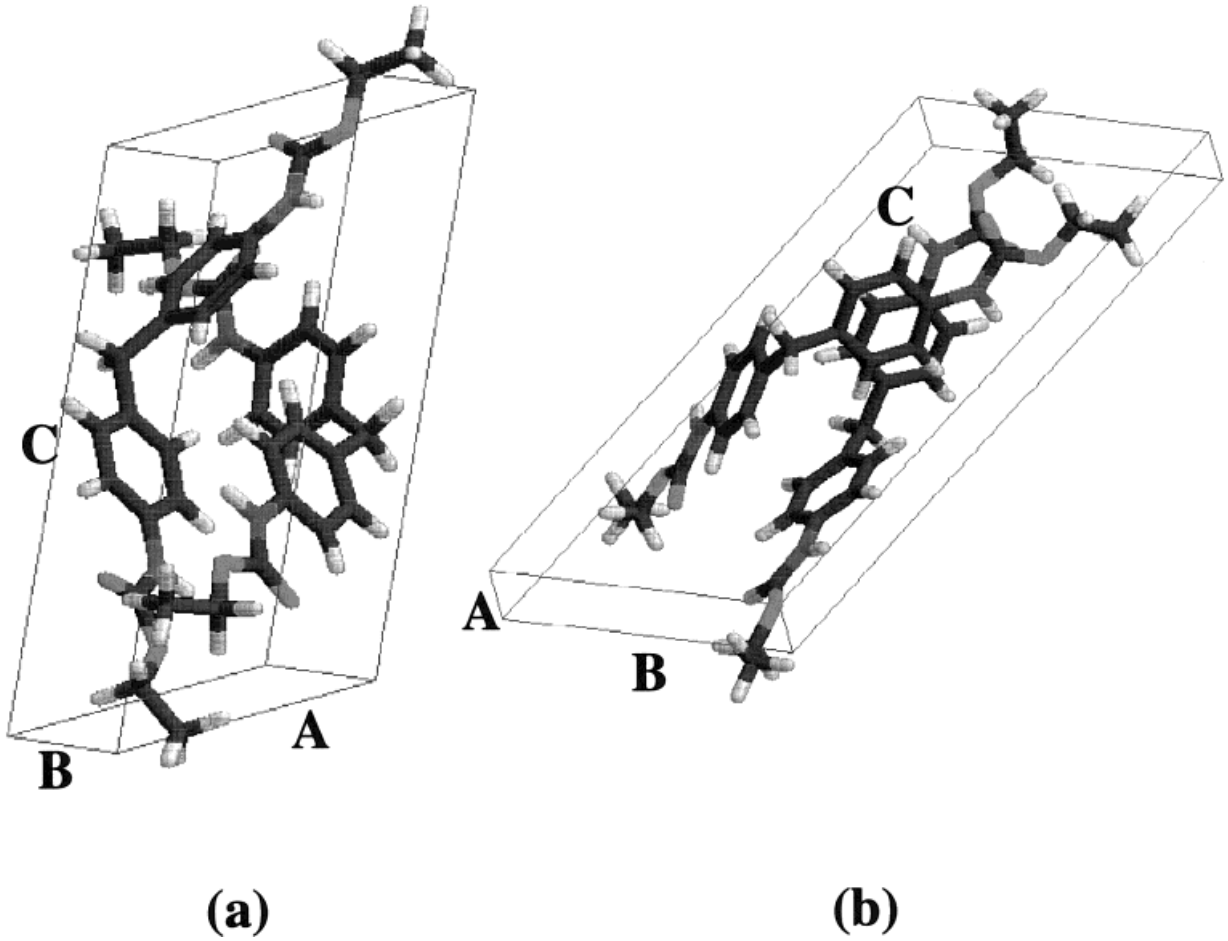

Figure 8. Crystal made from unconnected double helices with no hydrogen bonding. Cell length is about half that of hydrogen-bonded crystal of Figures 4 and 5. (a) and (b) represent two different views of the unit cell. Energies and crystal structure are given in Table I (column 7).

conformations in order to compare them to experimental data. The calculated energies for the two crystals differ by about 2 kJ/mol, well within the accuracy of the calculations, and are lower than all other calculated conformations by about 20 kJ/mol. One crystal was strongly hydrogen bonded between strands while the other formed a double helix with only van der Waals bonding.

Our procedure, finding the minimum energy conformation, differs fundamentally from previous methods that attempted to infer the crystal structure from observed fiber X-ray diffraction pattern. The interpretation of fiber diffraction patterns of MDI/BDO is difficult because of the ambiguity in assigning Bragg lines to the data and because the samples can be mixtures of several polymorphs of MDI/BDO. The main difficulty

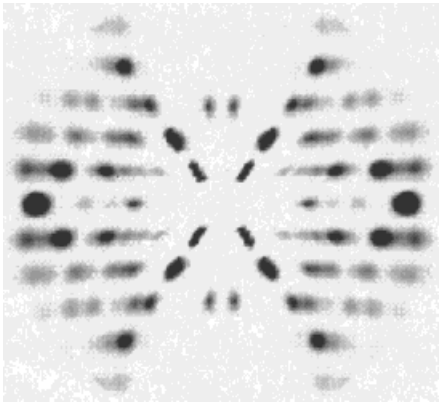

Figure 9. X-ray fiber pattern of crystal made from unconnected double helices in Figure 7.

in our procedure is that we cannot be certain that we have determined the absolute energy minimum (i.e., that we have examined all possibilities of molecular orientation and crystal cells). Despite this drawback, the fiber X-ray patterns calculated for our crystal conformations do show reasonable agreement with the observed X-ray pattern. The hydrogen-bonded crystals give rise to calculated patterns near the horizontal quite similar to observations, but have a (004) peak at 23° instead of 37 at $d = 8.0$ Å instead of $d = 7.6$ Å. Also, the calculations predict weaker peaks at (001), (002), and (003), which are not seen in the experimental data. The double helix crystal gives rise to fiber X-ray diffraction (002) peaks at exactly 37° and $d = 7.5$ Å, but the predicted (001) line at $d = 3.75$ Å is not observed experimentally, nor does the double helix crystal account for other peaks near the horizontal.

It is interesting to note that, before crystallization occurs in the hard segments, the MDI/BDO units are likely to be in double helix dimers as this conformation is about 38 kJ/mol lower in energy than any other hydrogen-bonded pair. This suggests that before a hydrogen-bonded crystal can form, the temperature must be increased to separate the double helices already formed This may provide an explanation for the high annealing temperatures required to create Type III crystals. Also, the two hard segment endotherms observed in the differential scanning calorimetry[14,17] data could arise from double helix crystals where one endotherm would correspond to the short-range helical structure and the other endotherm to the long-range crystal structure. Finally, the small-angle X-ray data of Koberstein and Stein[16] indicate that the hard segments form in sheets due to chain folding. It appears that the shorter crystal cell of the double helix conformation would be ideally suited to form sheets if the cells were only connected by one strand instead of two so that the fibers were folded along the c-axes. In this case, one would not expect to see c-axis layer lines originating from long double helix fibers.

The authors would like to thank Dr. Russell Pack for many interesting discussions and suggestions. This work was partially carried out under the auspices of the Los Alamos Laboratory Directed Research and Development program.

REFERENCES AND NOTES

1. Bonart, R. J Macromol Sci Phys 1968, 132, 115.
2. Bonart, R.; Morbitzer, L.; Hentze, G. J Macromol Sci Phys 1969, B3, 337.
3. Bonart, R.; Morbitzer, L.; Muller, E. H. J Macromol Sci Phys 1974, B9, 447.
4. Gardner, K. H.; Blackwell, J. Acta Crystallogr 1980, B36, 1972.
5. Forcier, P. G.; Blackwell, J. Acta Crystallogr 1981, B37, 286.
6. Blackwell, J.; Quay, J. R.; Nagarajan, M. R. J Polym Sci: Polym Phys Ed 1984, 22, 1247.
7. Blackwell, J.; Ross, M. J Polym Sci: Polym Lett 1979, 17, 447.
8. Blackwell, J.; Nagarajan, M. R.; Hoitink, T. Polymer 1981, 22, 1534.
9. Born, L.; Hespe, H.; Crone, J.; Wolf, K. H. Colloid Polym Sci 1982, 260, 819.
10. Born, L.; Crone, J.; Hespe, H.; Muller, E. H.; Wolf, K. H. J Polym Sci: Polym, Phys Ed 1984, 22, 163.
11. Quay, J. R.; Sun, Z.; Blackwell, J.; Briber, R. M.; Thomas, E. L. Polymer 1990, 31, 1003.
12. Leung, L. M.; Koberstein, J. T. J Polym Sci: Polym Phys 1985, 23, 1883.
13. Briber, R. M.; Thomas, E. L. J Macromol Sci Phys 1983, B22, 509.
14. Blackwell, J.; Lee, C. D. J Polym Sci: Polym Phys Ed 1984, 22, 759.
15. Briber, R. M.; Sung, P. Polym Commun 1987, 28, 162.
16. Koberstein, J. T.; Stein, R. S. J Polym Sci: Polym Phys Ed 1983, 21, 1439.
17. Koberstein, J. T.; Galambos, A. F. Macromolecules 1992, 25, 5618.
18. Blackwell, J.; Gardner, K. H. Polymer 1979, 20, 13.
19. Blackwell, J.; Nagarajan, M. R. Polymer 1981, 22, 202.
20. Blackwell, J.; Nagarajan, M. R.; Hoitink, T. B. Polymer 1982, 23, 950.
21. Sun, H. Macromolecules 1993, 26, 5924.
22. Discover 2.9.8/96.0/4.0.0 User Guide, Part 1: Forcefield Simulations (Molecular Simulations, Inc., San Diego, September 1996); Polymer User Guide, Release 4.0.0 (Molecular Simulations, Inc., San Diego, September 1996). Energy optimizations were performed with the Discover® program using the *cvff* force fields and graphics produced with the InsightII® molecular modeling system.